Vol. XX — No. 3 September, 1975

The SPEX INDUSTRIES, INC. · 3880 PARK AVENUE · METUCHEN, N.J.,08840 · ☎ (201)-549-7144

Speaker

RAMAN AND INFRARED INVESTIGATIONS OF OH^- AND H_2O IN HYDROTHERMAL α-QUARTZ

G. E. Walrafen[x] and J. P. Luongo
Bell Laboratories
Murray Hill, New Jersey 07974

SINCE Nacken [1] first succeeded in growing large single crystals of α-quartz hydrothermally in Germany during World War II, synthetic quartz has largely replaced natural quartz in numerous electronic devices. One reason for this is the rising scarcity of the natural material, the Brazilian government having imposed restrictions on its export just this year. But an even more important reason is economic: conversion of the raw material to finished crystals is less expensive for synthetic than for natural quartz. Technological developments at Bell Laboratories and Western Electric [2] and elsewhere [3] have resulted in the production of large, untwinned, preoriented crystals. In contrast, even the clearest natural quartz does not consist of single crystals. Instead, many regions of twins occur, which are worthless piezoelectrically, and must be removed.

The piezoelectric property of quartz, that is, its ability to convert mechanical energy into electrical energy (or vice versa), is its principle electronic feature. Today, highly stable oscillators of synthetic quartz are employed, for example, in the circuitry of every digital watch. And, a synthetic quartz crystal is used in each broadcast channel of every "walkie-talkie." In telephony, thousands of quartz crystals are manufactured each year, to be put into service as carrier oscillators and filters. For most of these applications the ordinary grade of hydrothermally-grown, synthetic quartz is suitable. However, in more exacting applications—repeaters in trans-oceanic cables, reference frequency standards—premium-quality quartz is required. Quality largely hinges on an inherent property of the material termed "Q." Infrared and Raman spectroscopy can detect impurities in the crystal lattice, which, in turn, are related to Q.

Q is an inverse measure of the quality of the crystal. During the process of energy conversion, a small amount of mechanical energy is converted, not to electronic energy, but to heat. This occurs because crystal imperfections give rise to internal friction when the crystal vibrates. But loss of conversion efficiency is only one factor. Another problem associated with high internal friction is that the mechanical resonance of the crystal will be broad. That is, the range of frequencies that excite mechanical resonance in the crystal will be large, a generally undesirable trait. While crystals with a Q of around 500,000 are more than adequate for most purposes, synthetic crystals with a Q approaching 3,000,000 are needed for some applications.

Defects such as OH^- and H_2O are known to lower the mechanical Q of quartz [4]. However, the laboratory synthesis of quartz commonly involves aqueous solutions of hydroxides, and thus, the synthetic crystals nearly always contain OH^- and H_2O, whereas OH^- is usually absent in natural quartz, which can have a very high Q, and the H_2O content is relatively much lower. Accordingly, an understanding of the nature of the defects is important in that improved methods of increasing the Q value of hydrothermal quartz could result.

In the present work, polarized Raman and polarized infrared investigations of OH^- and H_2O in hydrothermal α-quartz were conducted. These spectroscopic studies led to interesting structural implications involving the geometrical distribution of OH^- and H_2O defects in quartz, as well as to information related to the interactions between the OH^- and H_2O impurities. The Raman and infrared results are now presented.

EXPERIMENTAL

Polarized infrared transmittance spectra were recorded in the 4000 - 2500 cm^{-1} region with a Perkin-Elmer Model 421 double-beam grating spectrometer, using a silver wire grid polarizer. Samples of quartz 2 mm thick were cut from three faces of the crystal perpendicular to the x, y, and z axes. These axes are defined in Fig. 1. The directions of the infrared beam, relative to the orientation of the crystal, are designated I_0-X, I_0-Y or I_0-Z. The symbols $E_\perp$ and $E_{||}$ refer to the polarization of the infrared radiation used to record the spectra indicated in Fig. 2. In these experiments, the $E_\perp$ radiation is that for which the electric vector component passed by the wire grid polarizer is perpendicular to the (vertical) slits of the spectrometer and also perpendicular either to the seed plane of the crystal or to the y-axis. Rotation of the wire grid polarizer by 90° results in polarized radiation having its electric vector parallel to either the seed plane or the y-axis. It should be emphasized that in the present experiments, the unpolarized radiation from the spectrometer source passed through the

[x]Present address: Department of Chemistry, Howard University, 525 College St., N.W., Washington, D.C., 20059.

quartz sample first, and then through the wire grid polarizer. The polarizer is located inside the instrument at the crossing point of the sample and reference beams.

In connection with this, it is known that quartz rotates the plane of polarization of radiation propagated along the optic axis. Thus, in addition to the 2 mm thick sample, a thinner, 0.4 mm thick, sample was examined along the z-axis. It was found that the 0.4 mm thick sample gave the same polarization results as the 2 mm thick sample. Thus, optical rotation was not a problem for z-axis propagation.

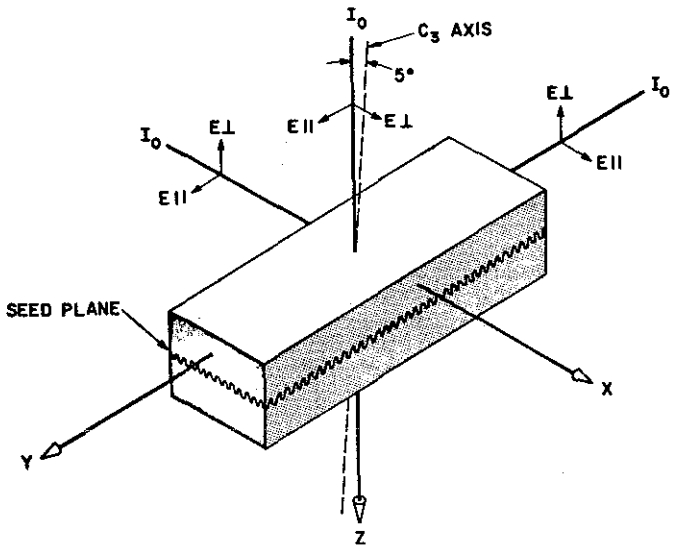

Figure 1. Seeded quartz crystal showing relative orientations of the x-, y- and z-axes.

Figure 1 also indicates that the true optic axis actually deviates from the z-axis by 5° in the XZ plane. This deviation resulted because the crystal was cut for device purposes. However, for simplicity, subsequent diagrams will show the optic and z-axes to be the same.

Raman spectra in the region of 4000 $cm^{-1} > \Delta\bar{\nu} > 2500$ cm^{-1} were obtained with a Spex Ramalog instrument. The Spex Ramalog is a double-monochromator instrument with holographic gratings, and photon-counting detection employing a cooled RCA C31034 photomultiplier tube. The sensitivity of this instrument is such that polarized Raman spectra of OH^- and H_2O impurities in hydrothermal α-quartz could readily be obtained with signal-to-noise ratios as high as 10 or 25 to 1 for the α_{zz}, α_{yy}, and α_{xx} spectra when the OH content was as low as 220 ppm. (Use of the computerized version of the Spex Ramalog should make it possible to study OH contents as low as 20 ppm or less by virtue of various data storing and averaging routines.) Slit-widths of 15 cm^{-1} were used with laser power-levels of 1.5 W. at 514.5 nm. A Polaroid analyzer was employed with a polarization scrambler to obtain the polarized Raman spectra from the oriented crystal. In the polarized Raman work the methods and nomenclature of Scott and Porto [5] were employed. For example, the symbol X(YX)Y means that the laser beam is in the X direction and its electric vector (Y in the Y direction, and that scattered radiation having its electric vector X) in the X direction is observed along Y. Because of optical activity along Z, however, it was essential to pass the focussed laser beam as near to the crystal surface as possible, when scattering was observed along the z-axis, i.e., when the X(YY)Z and Y(XX)Z configurations were employed. In addition, no measurements were attempted whatever with the laser radiation propagating along the z-axis, because the same information sought from Z excitation using Z(YX)Y, could be obtained by the orientation X(YX)Y. [5] For decompositions of some Raman spectra a duPont 310 Curve Resolver, a 10-channel analog computer capable of employing Gaussian or Lorentzian component shapes, was also employed.

The sample of hydrothermal α-quartz, X257-23, was studied previously. [6] It was grown in an aqueous KOH solution in a silver tube. The OH content, most probably exclusive of OH^-, was determined to be 220 ppm. [6] After slices were cut for infrared examination, the crystal was polished on all surfaces. Although the optic and z-axes deviated by 5° as mentioned, no attempt was made to remove this difference in the polishing process because it was thought not to be of great importance even for polarized Raman work.

POLARIZED SPECTRA

Polarized infrared spectra, $E_\perp$ and E_{II}, are shown in Fig. 2 for three orientations defined in Fig. 1, I_0-Z, I_0-X, and I_0-Y. In Fig. 2, a, b, and c, correspond to I_0-Z, I_0-X, and I_0-Y, respectively. Examination of Fig. 2, however, indicates that only two general classes of spectra are involved. These are called dichroic and nondichroic in this work. The I_0-Z spectra constitute the nondichroic class for which $E_\perp$ and E_{II} spectra are identical within experimental error, whereas the I_0-X, and I_0-Y spectra constitute the dichroic class for which the same differences are observed when $E_\perp$ and E_{II} radiation is used.

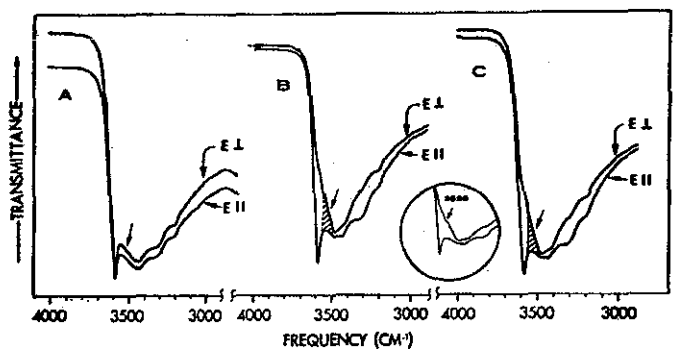

Figure 2. Polarized ($E_\perp$ and E_{II}) infrared spectra of quartz sample in the 4000 to 2500 cm-1 region. The designations a, b, and c refer, respectively, to I_0 — Z, I_0 — X, and I_0 — Y, see Fig. 1.

All of the E_{II} spectra of Fig. 2 give evidence of a sharp intense absorption at 3585 cm^{-1}, and of an intense broad asymmetric absorption band near 3440 cm^{-1}. The sharp band at 3585 cm^{-1} is attributed to the OH^- ion hydrated by H_2O, [7] and the broad band at 3440 cm^{-1} to hydrogen-bonded H_2O molecules. [8] The shoulders near 3200 and 3300 cm^{-1} are characteristic of quartz spectra, but were not studied in the present investigation.

In the two $E_\perp$ spectra of the dichroic class, the sharp absorption at 3585 cm^{-1} is seen to be virtually absent. In view of the fact that the broad absorption at 3440 cm^{-1} shows no significant changes in any of the Fig. 2 spectra, it is evident that another component near 3520 cm^{-1} is also absent in the two $E_\perp$ dichroic spectra. The 3520 cm^{-1} component is evident as a shoulder in the inset where the wavelength scale was expanded by 2X. Further, the dichroic $E_\perp$ and $E_\parallel$ spectra show a difference at 3520 cm^{-1} which cannot be wholly accounted for by overlap of the absorptions at 3585 cm^{-1} and 3440 cm^{-1}. This difference is shown by the cross-hatched area. The 3520 cm^{-1} component is assigned to OH vibrations of H_2O molecules hydrogen-bonded to OH^- ions.

Polarized Raman spectra are shown in Figs. 3 through 6 in the Raman shift region from $\Delta\bar{\nu} \approx 4000 - 2500$ cm^{-1}. Diagrams showing the orientation of the crystal, the direction of the laser beam used for excitation, and the direction of observation are included (to the right) in all of the figures. The vertical laser beam is labeled in all cases, and the observation direction is shown by a long horizontal arrow at 90° to the laser beam. The electric vectors of the excitation and scattered radiation are shown by short arrows.

In Fig. 3 two Raman spectra are shown corresponding to the orientations X(ZZ)Y and Y(ZZ)X. Both of these orientations refer to the same tensor component of the polarizability, α_{zz} and within the experimental noise levels the spectra are seen to have the same shape. The intensity maximum indicated from Fig. 3 occurs near ~ 3450 cm^{-1}. In addition the spectra indicate a low-frequency tail suggestive of at least one broad unresolved component centered near ~ 3300 cm^{-1}. Further, a weak high-frequency shoulder is also evident near 3590 ± 15 cm^{-1}.

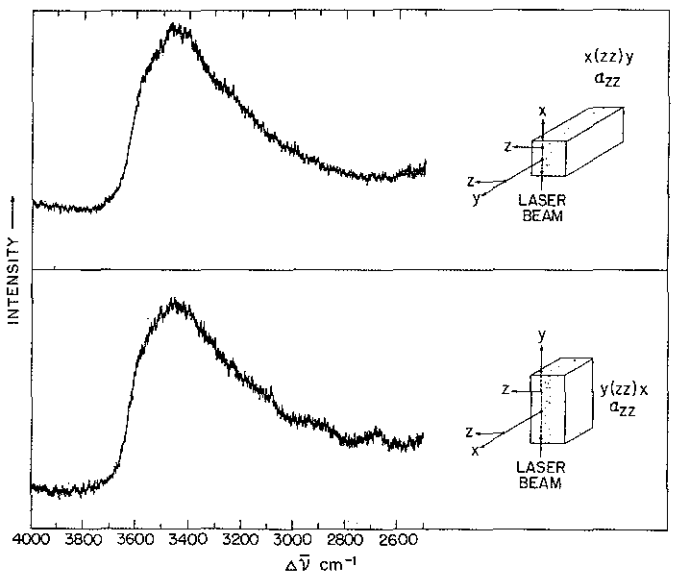

Figure 3. Raman spectra corresponding to α_{zz}.

Raman spectra corresponding to the two orientations X(YY)Z and Y(XX)Z are shown in Fig. 4. These orientations refer to the tensor components α_{yy} and α_{xx}. However, because the measurements involved observations along the z-axis, it was necessary to pass the exciting laser beam through the crystal as near to the surface as possible to prevent significant rotation of the plane of polarization of the scattered radiation. Within the experimental noise levels, the two spectra are seen to have the same shape, and thus α^2_{yy} and α^2_{xx} are equal. Symbols of the type α^2_{ik} used here, and subsequently, are shorthand for $\{[P^\circ]^{n,m}_i\}^2$, see Herzberg. [9] It should be noted that the Fig. 4 spectra possess an intense sharp maximum near 3590 cm^{-1}, as opposed to Fig. 3, where a similar feature is very weak. In addition, the Fig. 4 spectra show high intensity near ~ 3450 cm^{-1}, and they also give indications of another broad unresolved component in the region of 3300 cm^{-1}. Thus, the Fig. 4 spectra differ from the spectra of Fig. 3 primarily with regard to the intense sharp component at 3590 cm^{-1}. (A weak ~ 3525 cm^{-1} component discussed subsequently constitutes another difference.)

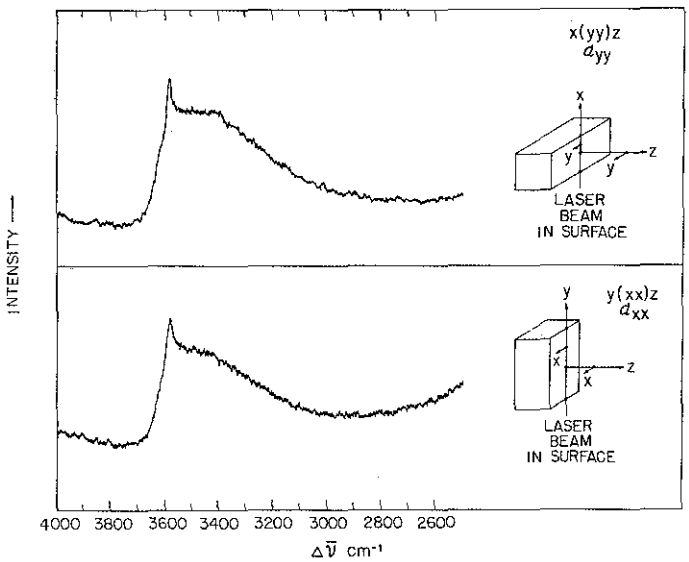

Figure 4. Raman spectra corresponding to α_{yy} (top) and α_{xx} (bottom).

Raman spectra corresponding to the X(ZX)Y, Y(XZ)X, X(YZ)Y, and Y(ZY)X orientations are shown in Fig. 5. Examination of Fig. 5 indicates that all of the spectra have the same shape within the experimental noise levels. In particular, spectra corresponding to X(ZX)Y and X(YZ)Y seem to be the most reliable of the four spectra, and they have essentially the same shapes. Thus $\alpha^2_{zx} = \alpha^2_{yz}$, and, of course, $\alpha_{zx} = \alpha_{xz}$ and $\alpha_{yz} = \alpha_{zy}$ Raman spectra corresponding to the Y(XY)X and X(YX)Y orientations are shown in Fig. 6 for comparisons with Fig. 5. Again $\alpha_{yx} = \alpha_{xy}$, and the spectral shapes are essentially the same. However, an additional weak component at about 3590 cm^{-1} is present, which is not evident in Fig. 5. Thus, Figs. 5 and 6 differ in the same qualitative manner in which Figs. 3 and 4 differ, namely in regard to a feature near 3590 cm^{-1}. These common differences between the two pairs of figures are very important, and can be explained by stating that the 3590 cm^{-1} component is either weak or absent when the polarizability tensor has at least one Z element. Thus, the 3590 cm^{-1} Raman component which previously was observed to change markedly in the infrared dichroic spectra, and which is considered to arise from hydrated OH^- ions, is associated primarily with the XY plane of the hydrothermal quartz.

Analog computer decompositions of the spectra of Figs. 3 and 6 was accomplished with a duPont analog computer. Gaussian component shapes were found to be completely adequate for all of the broad components, but not for the

narrow component at 3590 cm^{-1} which definitely required a Lorentzian component shape. The computer results are shown in Table I in which the Gaussian peak positions, $\Delta\tilde{\nu}$, are given.

Three, broad Gaussian components were found to decrease in peak height in the order 3490-3525, 3300-3350, and 3000-3050 cm^{-1}. (The $\Delta\tilde{\nu}_{1/2}$ values in the table refer to average values for all of the $\Delta\tilde{\nu}$ entries above.) A weak Gaussian component at 3525 cm^{-1} was only clearly indicated in the intense α_{xx} and α_{yy} spectra, where it was absolutely necessary to employ that component. The weak 3525 cm^{-1} Raman component has a counterpart in the infrared spectra at 3520 cm^{-1}, and was assigned previously to OH units of H_2O molecules hydrogen-bonded to OH^- ion. Similarly, the sharp Lorentzian component at 3590 cm^{-1} corresponds to the sharp 3585 cm^{-1} infrared component due to hydrated OH^- ion.

INTERPRETATION

Infrared spectra of solid LiOH and $LiOH{\cdot}H_2O$ have been reported. [7] The unhydrated OH^- ion gave rise to a sharp absorption at 3678 cm^{-1}, and the hydrated OH^- ion in the solid monohydrate yielded a sharp absorption at 3574 cm^{-1}. [7] In the present work, a sharp intensity maximum has been observed at 3590 cm^{-1} in the Raman spectrum, and a sharp absorption at 3585 cm^{-1} in the infrared spectrum. These features occur within ~ 10 cm^{-1} of the value reported for $LiOH{\cdot}H_2O$. Hence, they are assigned to hydrated OH^- ion in hydrothermal quartz.

Raman Gaussian components centered near 3000-3525 cm^{-1} have also been obtained in this work from computer analysis of Figs. 3 through 6, see Table I. Also, strong infrared absorption has been observed throughout the region corresponding to these Raman components, and a dichroic infrared component was also identified at 3520 cm^{-1} in reasonable agreement with a weak Raman component near 3525 cm^{-1}. The three other components centered in the region of 3000-3525 cm^{-1} are assigned to various vibrations of H_2O molecules engaged in various kinds of hydrogen bonding. The 3520 cm^{-1} dichroic infrared and 3525 cm^{-1} Raman components are assigned to OH groups of H_2O molecules hydrogen-bonded to OH^- ion.

The infrared spectra of Fig. 2 corresponding to I_0-X and I_0-Y orientations indicate dichroism for the 3520 and 3585 cm^{-1} components. Thus, it is evident that the corresponding hydrogen-bonded O-H···O-H$^-$ structures lie in (XY) planes perpendicular to the optic (Z) axis of the hydrothermal quartz. The presence of the O-H···O-H$^-$ structures in planes perpendicular to the optic axis indicates that the defect orientations are influenced by the D_3 crystal symmetry. The I_0-Z spectra of Fig. 2, however, show no dichroism. This lack of dichroism suggests orientational possibilities for the O-H···O-H$^-$ groups such as D_{3h} or C_s, where the D_{3h} symmetry arises from the C_3 axis of the D_3 quartz structure and the simultaneous presence of XY planes, and where the C_s symmetry refers to more or less random orientations of the O-H···O-H$^-$ groups in the XY planes.

The broad infrared components of Fig. 2 in the region below 3520 cm^{-1} show no evidence of dichroism. This region was assigned to hydrogen-bonded H_2O molecules, and the orientations of these molecules therefore is probably random.

Table I

α_{ij}	Raman Shift at Component Center, $\Delta\tilde{\nu}$ cm^{-1}				
α_{xz} or α_{yz}	—	—	3525 +15	3350 ±25	3050±75 (weak)
α_{xy}	3590 ±5	—	3510 ±15	3350 ±25	3050±75 (weak)
α_{xx} or α_{yy}	3590 ±5	3525±10 (weak)	3510 +15	3350 ±25	3050±75 (weak)
α_{zz}	3590 ±5 (weak)	—	3490 ±15	3300 ±25	3000±75 (weak)
Half width $\Delta\tilde{\nu}$½ cm^{-1}	~50	~125	~200	~350	~350

Analog computer decompositions of the Raman spectra of Figs. 3 through 6 indicate three broad components common to all of the spectra. These three components are centered from about 3000-3525 cm^{-1}. Because these components are thought to be related to vibrations of randomly oriented H_2O molecules, it is reasonable that, if Raman active by virtue of the selection rules for H_2O, or through violations of those selection rules, they would be represented in spectra referring to all of the six tensor quantities involved in Figs. 3 through 6. The combined 3525 and 3585 cm^{-1} components, however, are intense in Fig. 4 where no Z component is involved. This is readily explained. The O-H···O-H$^-$ structures lie in the XY planes, and it is generally accepted that the largest polarizability changes occur along the bond directions. Hence, Raman intensities of O-H and O-H$^-$ in the O-H···O-H$^-$ structures would be large for α_{xx} and α_{yy}, which involve the XY planes. (Of course, weak Raman intensity was observed near 3590 cm^{-1} in Fig. 3 which refers to α_{zz}, but this could arise because a small part of the polarizability change occurs perpendicular to the bond direction. (The z- and optic axes also differed by 5 degrees, which could lead to some contributions from α_{xx} for which the 3590 cm^{-1} component is very intense.)

In accord with the infrared observations, it is possible to explain some of the Raman observations (from Fig. 4, $\alpha^2_{xx} = \alpha^2_{yy}$, or from Fig. 5, $\alpha^2_{zx} = \alpha^2_{xy}$) in terms of D_{3h} or C_s symmetry, because for these symmetries $\alpha_{xx} = \alpha_{yy}$ and $\alpha_{zx} = \alpha_{zy}$, for non-degenerate vibrations. [10] However, a point of view involving isolated OH^- ions and isolated H_2O molecules, and perturbations of them, is probably more instructive, and also agrees with the infrared observations.

For an isolated OH^- ion, the derivative of the cross-tensor component with respect to the normal coordinate, $(\partial\alpha_{ik}/\partial q_i)_0$, where $i \neq k$, is zero. Similarly, for H_2O of C_{2v} symmetry, $(\partial\alpha_{ik}/\partial q_i)_0$, $i \neq k$, is zero for the totally symmetric

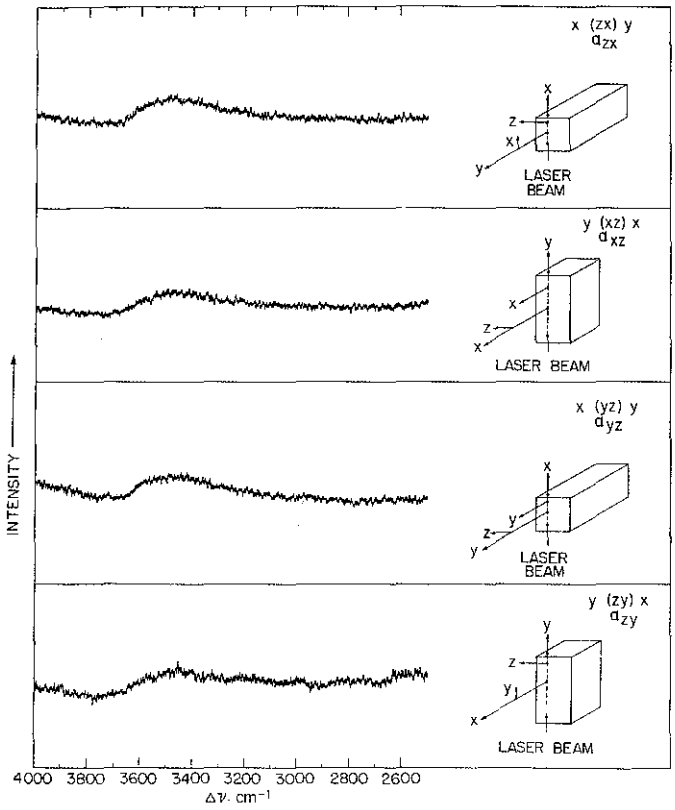

Figure 5. Raman spectra corresponding to α_{zx} and α_{xz} (top two), and to α_{yz} and α_{zy} (bottom two).

motions, and it is only non-zero for the in-plane cross-tensor component for asymmetric stretching, v_3. (But v_3 for H_2O is probably weak in all of the present Raman spectra.) On the other hand, all of the derivatives of the symmetric tensor components for OH^- and H_2O are non-zero for totally symmetric motions. Hence, if the OH^- ions lie in the xy planes, and in random orientations, $\alpha^2_{xx} = \alpha^2_{yy}$, and α^2_{zz} is small but finite. (Similar considerations would apply to just the OH part of the water that is hydrogen bonded to OH^-, and in the xy plane). These considerations explain the high and equal intensities at 3590 cm^{-1} in Fig. 4, as well as the small intensity at that position in Fig. 3. But they do not explain why the 3590 cm^{-1} component occurs in Fig. 6, because the cross-tensor derivatives are zero. However, if, for example, cations lie in the xy planes near the OH^- ions such that they perturb the electronic charge distributions more or less perpendicularly to the bond axis, then α_{xy} could become small and finite at 3590 cm^{-1}, as observed. (The cations might be too far apart between planes to affect α_{zx} and α_{zy}.) Further, for liquid water where a random tetrahedral hydrogen-bonded network is involved, it is known that the cross-tensor derivatives are non-zero for totally symmetric motions, in violation of the expectations for isolated H_2O molecules. [11] Thus, some off-plane non-symmetric perturbations, such as might arise from random tetrahedral hydrogen bonding, may be involved, and from the experimental liquid water results, one would expect that all of the Raman intensities due to random water in Figs. 5 and 6 would be small and equal, as is in fact observed. Also, for random orientations of H_2O molecules one would expect all of the symmetric tensor component derivatives to be equal for the symmetric stretching motion. From Fig. 4, it is evident that $\alpha^2_{xx} = \alpha^2_{yy}$. Further, it is very likely that $\alpha^2_{xx} = \alpha^2_{yy} = \alpha^2_{zz}$, when it is considered that part of the laser beam was lost through surface passage in the case of Fig. 4, see diagrams. This would make the Fig. 4 intensities just a little lower than those of Fig. 3, as observed for the main component of the random water, near 3450 cm^{-1}.

With regard to the conclusion that the O-H···O-H$^-$ units lie in xy planes perpendicular to the z or optic axis, it should be stated that the D_3 crystal symmetry might yield a disposition toward D_{3h} defect symmetry. But the OH^- content is probably much lower than 220 ppm. Hence, even if D_{3h} symmetry were favored, missing O-H···O-H$^-$ units would yield C_s symmetry. Or, if some O-H···O-H$^-$ units were rotated relative to each other, D_{3h} symmetry would quickly yield C_s symmetry; and, C_s symmetry seems favored when all of the spectroscopic data of this work are considered. In addition, some further comments relative to the defects need to be made.

The H_2O to OH^- ratio of the hydrothermal quartz studied is estimated to lie between the extremes of 1 and 7. [12] However, an examination of the α-quartz structure indicates that there is almost certainly insufficient space to accommodate such aggregates of OH^- ions and H_2O molecules within the crystal lattice. Therefore, although the D_3 crystal symmetry may be important in determining the orientations that the defects will assume, it is reasonable to postulate that considerable disruption of the crystal structure must occur near such large defects.

The hydrothermal quartz studied in this work was grown from an aqueous KOH solution in a silver tube. It is reasonable to expect, therefore, that K^+ ions or hydrated K^+ ions were incorporated into the hydrothermal crystal, and some suggestive evidence relative to the K^+ ions was evident from this work. (Ag^+ ions could also be involved.) Further, the present Raman and infrared data are consistent with a picture involving defects such as $OH^-(H_2O)_n$, where most of the OH groups of the $(H_2O)_n$ are randomly oriented. Of course, the present data are also consistent with other types of defects such as $OH^-(H_2O)$ and $(H_2O)_{n-1}$, where $(H_2O)_{n-1}$ refers to randomly oriented water molecules on separate sites. This picture could be further complicated by taking the cations into consideration.

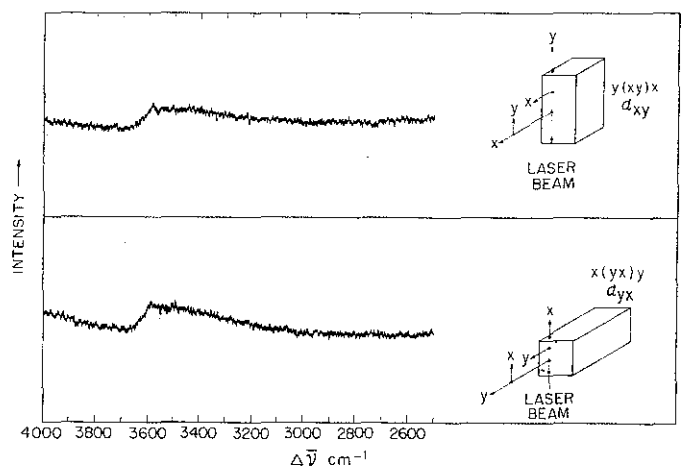

Figure 6. Raman spectra corresponding to α_{xy} (top) and α_{yx} (bottom).

Finally, it should be mentioned that there can be little doubt that the water in hydrothermal quartz exists as H_2O molecules, as opposed to the Si-OH groups that occur in fused silica. The Raman OH stretching region of fused silica was recently examined, and a Raman band near 3690 cm^{-1} was observed and assigned to Si-OH groups. [13] However, no significant intensity is evident in Figs. 3 through 6 near 3690 cm^{-1}, and therefore Si-OH groups must be essentially absent. Accordingly the water in the hydrothermal quartz studied, although hydrogen bonded in various ways, must refer to H_2O molecules.

SUMMARY

Hydrothermal α-quartz containing OH^- and H_2O impurities was investigated using polarized Raman and infrared techniques. The polarized infrared studies of oriented sections yielded dichroic and nondichroic spectra, and the corresponding Raman studies yielded spectra related to the six tensors $\alpha_{xx'}$ $\alpha_{yy'}$ $\alpha_{zz'}$ $\alpha_{xy'}$ $\alpha_{xz'}$ α_{yz}. The combined Raman and infrared data indicated that hydrogen-bonded O-H · · · O-H$^-$ units of hydrated OH^- ions lie in planes perpendicular to the optic axis of the quartz. Hydrogen-bonded aggregates of H_2O molecules, however, occur in random orientations, and it is probable, but not completely certain, that the randomly oriented H_2O aggregates are common to the hydrated OH^- structure.

ACKNOWLEDGMENTS

The authors wish to thank H. D. Keith and D. J. Freed for suggesting the present problem. In addition, special thanks are due to D. L. Wood for supplying the hydrothermal quartz sample, and for numerous helpful discussions. The authors are also grateful to E. A. Sigety for cutting and polishing the quartz crystals.

REFERENCES

1. R. Nacken, Office of Technical Services Reports, PB 6,498; PB 18,784; PB 28,897. Dept. of Commerce, Washington, D. C. See also E. Buehler and A. C. Walker, Scientific Monthly, *LXIX*, 148 (1949).
2. A. A. Ballman and D. W. Rudd, Western Electric Engineer, p. 3, Jan. 1965; D. W. Rudd, E. E. Houghton, and W. J. Carroll, ibid., p. 22, Jan. 1966; N. C. Lias and D. W. Rudd, ibid., p. 23, April 1969.
3. For example, at the Clevite Corporation, Cleveland, Ohio.
4. D. B. Fraser, D. M. Dodd, D. W. Rudd, and W. J. Carroll, Frequency *4*, 18 (1966).
5. J. F. Scott and S. P. S. Porto, Phys. Rev. *161*, 903 (1967).
6. A. A. Ballman, D. M. Dodd, N. A. Kuebler, R. A. Laudise, D. L. Wood, and D. W. Rudd, Appl. Optics *7*, 1387 (1968).
7. L. H. Jones, J. Chem. Phys. 22, 217 (1954).
8. G. E. Walrafen, chapter in "Water: A Comprehensive Treatise. Vol. I. The Physics and Physical Chemistry of Water," (Plenum, New York, 1972), pgs. 151-214.
9. G. Herzberg, "Infrared and Raman Spectra," (Van Nostrand, New York, 1945).
10. G. F. Koster, J. O. Dimmock, R. G. Wheeler, and H. Statz, "Properties of the Thirty-Two Point Groups," (M.I.T. Press, Cambridge, 1963).
11. G. E. Walrafen, in "Structure of Water and Aqueous Solutions," edited by W. Luck (Verlag Chemie, Weinheim, 1974).
12. The Raman spectrum from a saturated aqueous solution of LiOH having an $[H_2O]/[OH^-]$ ratio of $\sim$ 10.3 was obtained. This spectrum was then compared with a Raman spectrum from hydrothermal quartz obtained in the comparable [X(YY)Z + X(YX)Z] orientation. The integrated Gaussian component intensity ratio of the 3460 and 3620 cm^{-1} components from the solution, was compared with the corresponding ratio of the $\sim$ 3500-3525 cm^{-1} and $\sim$ 3585 cm^{-1} components from the crystal. From this very rough comparison it was concluded that the upper limit of the $[H_2O]/[OH^-]$ ratio for the crystal may be near 7.
13. G. E. Walrafen, J. Chem. Phys. *62*, 297 (1975).

ACCESSORIES FOR RAMAN EXCITATION OF SOLIDS

D. N. Waters, School of Chemistry, Brunel University
Uxbridge, Middlesex. U.K.

THE 90° scattering geometry, a feature of the Spex model 1430 Raman Sample Illuminator (and its successors) has established itself as generally the most convenient and versatile technique for the excitation of Raman samples. A variety of standard accessories permits the investigation of substances in all states of aggregation and under a variety of conditions. Solid samples in the form of microcrystalline or amorphous powders are often examined in capillary tubes and excellent spectra can generally be obtained. With such samples an interference or Claassen filter is required in the incident laser beam to remove unwanted atomic lines, since the intensity of scattered radiation of unshifted frequency ("Rayleigh" light) is usually high.

We have found that this technique sometimes gives problems when solids have to be examined whose Raman spectra are rather weak. Some polymeric materials and samples of biochemical origin fall into this category. Reflections from the glass of capillary tube can both increase the amount of unwanted laser radiation entering the spectrometer and can reduce the intensity of collected Raman light. (The first effect is probably accentuated if, as is often the case, the electric vector of the incident beam is oriented parallel to the tube axis). In addition, although the Raman spectrum of glass (or silica) is relatively weak, bands arising from the material of the capillary can sometimes be seen in the spectra (a moderately sharp band near 180 cm^{-1} and a broad, weaker feature at 300-500 cm^{-1}) and might be confused with bands of the sample.

For these reasons we often prefer to avoid glass containers when recording the Raman spectra of solids. A simple 'home-made' accessory which achieves this is sketched in Fig. 1. It consists of a short length of stainless steel rod with a flat milled at the lower end at an angle of about 35° to the rod axis. Centrally in this flat face is a small drilled cavity (of about 1/8" diameter and 1/16" depth). The rod is mounted by means of a short threaded section (which can be used for height adjustment) into a larger diameter support, and the whole may be installed simply in the Spex standard holder for 1 cm^3 liquid cells, a basic accessory of the sample illuminator. In use the powder, finely ground, is pressed into the cavity with a small spatula and the sample holder is then located in position in the 1 cm^3 liquid cell holder. Several instances of spectra superior in quality to those obtained with capillary tubes have been recorded with this device.

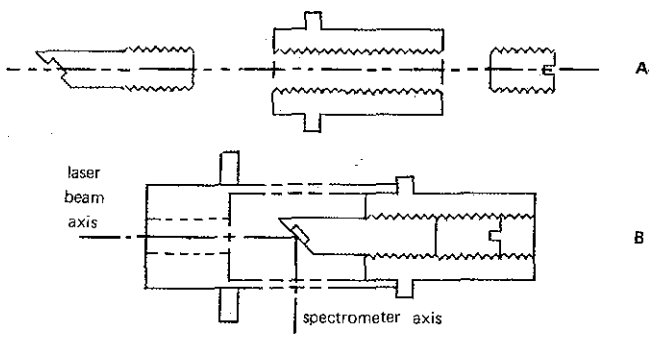

Figure 1. Powdered solids holder for oblique incidence.

(a) Components: locking screw (top), sample holder body (centre), rod with drilled cavity for sample at its lower end (bottom).

(b) Sample holder mounted in Model 1430 liquid cell holder.

Another problem that can arise with some solids is overheating and subsequent decomposition at the focus of the laser beam. When not restricted by sample size, the use of a sample spinning accessory can avoid this difficulty, but this procedure will not always overcome problems of residual fluorescence, which can best be quenched out if the sample remains static. With smaller, static samples, defocusing the laser beam can be helpful, but then only a proportion of the illuminated region of the sample can be imaged onto the monochromator entrance slit. A method which permits more efficient matching of the illuminated area to the monochromator optics, and which is especially suitable for use in conjunction with the front-surface illumination technique described above, involves a cylindrical lens in the laser beam.

The standard lens for focusing the laser beam in the model 1430 Illuminator has a focal length of 30 mm. The lens is mounted at the top of a short tube with facilities for focusing. In our adaptation (see Fig. 2), we mount a planoconcave cylindrical lens of focal length 120 mm immediately above the standard lens. The effect of this is to produce a line focus, instead of a point focus of the laser beam. The length of the line, for a 2 mm diameter laser beam, is approximately 0.5 mm. Rotation of the concave lens about a vertical axis allows the line focus to be aligned parallel to the spectrometer optical axis. If now a solid sample in the form of a flat disc or pellet is mounted at the focus, in the sloping orientation of Fig. 1, the line focus on the surface of the sample may be imaged by the scattered-light collection lens of the illuminator rather effectively at the entrance slit of the spectrometer.

Of course there will be slight degradation of sharpness of the line image, since the scattered radiation does not come from one point, but rather from a small range of distances in front of the Raman collection lens. Nevertheless, the collection efficiency is considerably improved over the simple, previously discussed alternative in which light is collected from a diffuse patch produced by defocusing the laser beam.

Finally it appears possible that the device could also be advantageous for Raman back-scatter measurements, e.g. with the model 1423A 180° Viewing Platform. Image degradation of the line focus should be negligible in such an arrangement, and excellent coupling with the spectrometer optics should result.

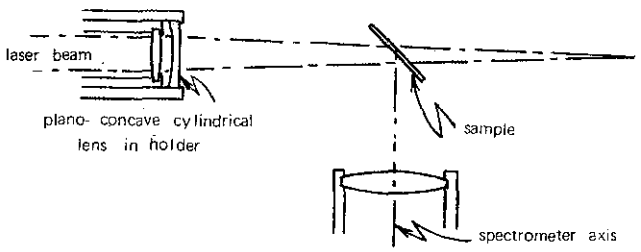

Figure 2. Arrangement of plano-concave cylindrical lens for producing a line focus of the laser beam at the surface of a solid sample.

SPEX

RAMALOG/RAMACOMP

LASER - RAMAN SYSTEMS

analyze almost anything

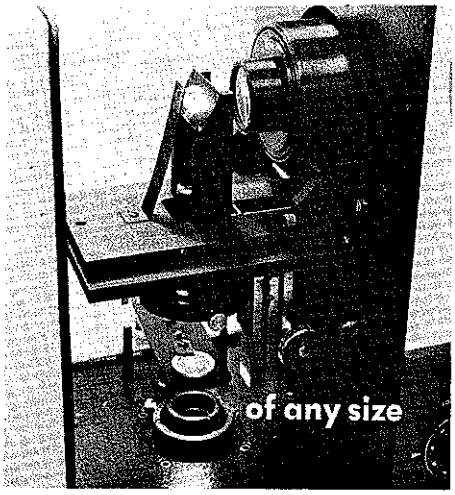

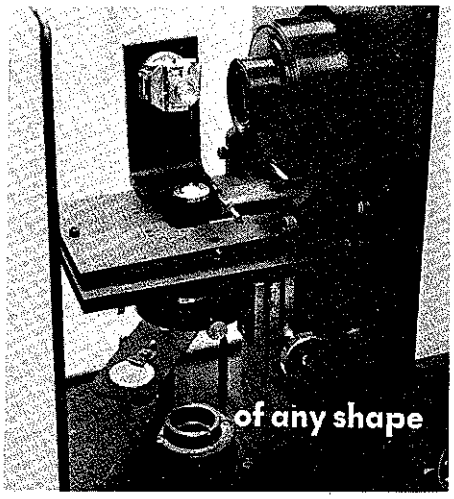

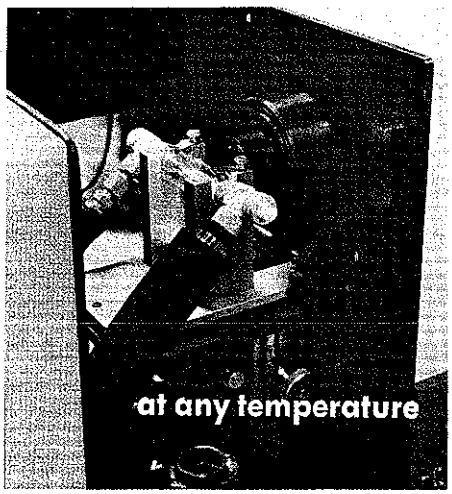

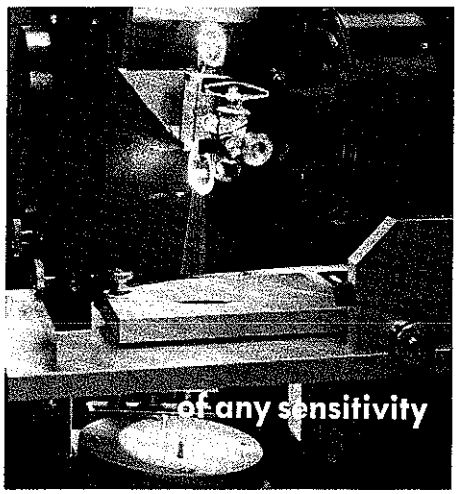

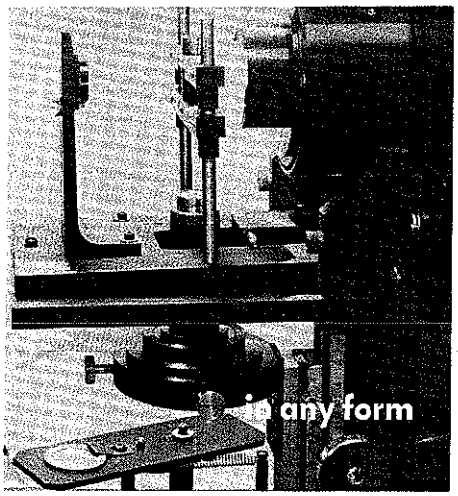

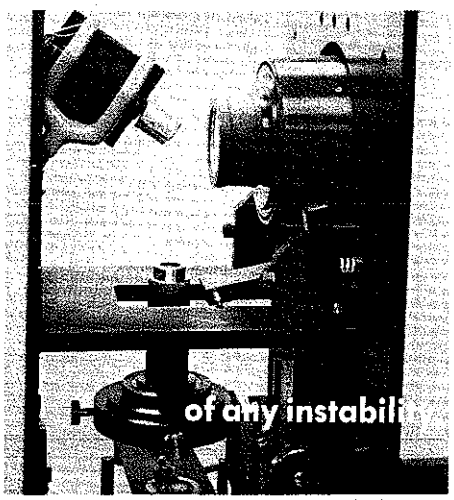

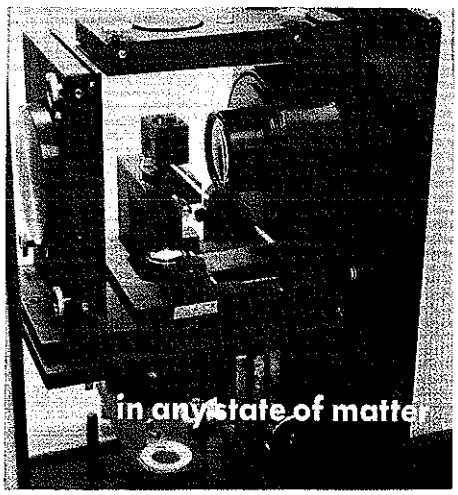

near or far . . . . .

OUR NEW CATALOG, BEING READIED, WILL BE MAILED FOR YOUR ASKING.

WESTERN REGIONAL OFFICE: 3246 McKINLEY DR., SANTA CLARA, CA. 95051 408/246-2333

SPEX INDUSTRIES INC./P.O. BOX 798/METUCHEN, N J 08840

BULK RATE/U. S. POSTAGE
PAID
Permit No. 166/ Plainfield, N. J.